IOP Publishing Plasma Physics and Controlled Fusion

Plasma Phys. Control. Fusion **56** (2014) 015009 (10pp) doi:10.1088/0741-3335/56/1/015009

Modulation of prompt fast-ion loss by applied $n = 2$ fields in the DIII-D tokamak

M A Van Zeeland[1], N M Ferraro[1], W W Heidbrink[2], G J Kramer[3], D C Pace[1], X Chen[2], T E Evans[1], R K Fisher[1], M García-Muñoz[4], J M Hanson[5], M J Lanctot[1], L L Lao[1], R A Moyer[6], R Nazikian[3] and D M Orlov[6]

[1] General Atomics, PO Box 85608 San Diego, CA 92186-5608, USA
[2] Department of Physics and Astronomy, University of California at Irvine, Irvine, CA 92697, USA
[3] Princeton Plasma Physics Laboratory, PO Box 451, Princeton, NJ 08543-0451, USA
[4] Max-Planck-Institut für Plasmaphysik, Euratom Association, Garching, Germany
[5] Department of Applied Physics and Applied Mathematics, Columbia University, New York, NY 10027, USA
[6] Energy Research Center and Mechanical and Aerospace Engineering Department, University of California San Diego, 9500 Gilman Dr., La Jolla, CA 92093-0417, USA

Received 21 August 2013, revised 18 October 2013
Accepted for publication 12 November 2013
Published 20 December 2013

Abstract

Energy and pitch angle resolved measurements of escaping neutral beam ions ($E \approx 80$ keV) have been made during DIII-D L-mode discharges with applied, slowly rotating, $n = 2$ magnetic perturbations. Data from separate scintillator detectors (FILDs) near and well below the plasma midplane show fast-ion losses correlated with the internal coil (I-coil) fields. The dominant fast-ion loss signals are observed to decay within one poloidal transit time after beam turn-off indicating they are primarily prompt loss orbits. Also, during application of the rotating I-coil fields, outboard midplane edge density and bremsstrahlung emission profiles exhibit a radial displacement of up to $\delta R \approx 1$ cm. Beam deposition and full orbit modeling of these losses using M3D-C1 calculations of the perturbed kinetic profiles and fields reproduce many features of the measured losses. In particular, the predicted phase of the modulated loss signal with respect to the I-coil currents is in close agreement with FILD measurements as is the relative amplitudes of the modulated losses for the co and counter-current beam used in the experiment. These simulations show modifications to the beam ion birth profile and subsequent prompt loss due to changes in the edge density; however, the dominant factor causing modulation of the losses to the fast-ion loss detectors is the perturbed magnetic field ($\delta B/B \approx 10^{-3}$ in the plasma). Calculations indicate total prompt loss to the DIII-D wall can increase with application of the $n = 2$ perturbation by up to 7% for co-current injected beams and 3% for counter-current injected beams depending on phase of the perturbation relative to the injected beam.

Keywords: tokamaks, spherical tokamaks, particle measurements, fusion products effects (e.g. alpha-particles, etc), fast particle effects, particle orbit and trajectory, plasma heating by particle beams

(Some figures may appear in colour only in the online journal)

1. Introduction

In tokamaks, energetic particles (EPs) play critical roles in heating, current drive, momentum input and plasma stability, making their successful confinement essential. Due to their relatively collisionless orbits and long confined path lengths; however, EPs are particularly sensitive to toroidal symmetry-breaking fields which can cause EP transport and potentially loss, the latter being a particular concern for device integrity [1]. These non-axisymmetric fields can come from any number of sources, including fields either intrinsic to a given device (error fields or ripple), MHD induced, or imposed by external coil systems. This letter focuses on the low toroidal mode number magnetic perturbations similar to that introduced

by coils intended to mitigate edge localized modes (ELMs). The possible implementation of ELM mitigation coils on ITER has motivated a number of recent calculations related to the effect of these magnetic perturbations on the confinement of 1 MeV neutral beam ions and 3.5 MeV alphas [2–5]. Some calculations predict EP losses in excess of 10%, challenging device integrity. The predictions are sensitive to the modeling of the plasma response to the magnetic perturbations, which can increase the perturbed field in some regions and decrease it in others. Experimentally, reasonable agreement has been reported between modeled fast-ion transport and signals from a loss detector in the ASDEX Upgrade tokamak [6, 7].

This paper describes the detailed analysis and modeling of an experiment designed to investigate fast-ion loss induced by internal coil (I-coil) imposed rotating $n = 2$ (n = toroidal mode number) magnetic perturbations in the DIII-D tokamak. In the experiment, loss of 80 keV injected beam ions was observed by two energy and pitch angle resolving fast-ion loss detectors (FILDs) located near the outboard midplane (FILD-mid) and significantly below the outboard midplane (FILD-low) [8–10]. The dominant loss signal observed by each detector was found to be due to prompt beam ion loss and the midplane FILD observed modulation of the prompt beam ion losses synchronized with the $n = 2$ fields. In the same discharges an approximately 1 cm radial oscillation of edge kinetic profiles was observed and it was not *a priori* obvious whether the dominant factor causing modulated loss to FILD-mid was due to modifications of the beam ion birth profile by the perturbed kinetic profiles or the field induced orbit perturbation caused the modulation. Modeling described here, that includes modification of the beam ion birth profile as well as the 3D fields with and without plasma response, as calculated by M3D-C1 [11–13], shows the dominant factor causing modulation of the losses to FILD-mid is the perturbed magnetic field. The same modeling reproduces many features of the measured losses including the phase of the modulated loss signal with respect to the I-coil currents as well as the relative amplitudes of the modulated losses for the co and counter-current beam used in the experiment. The simulated overall depth of modulation is smaller than observed experimentally and, because the depth of modulation predicted with the vacuum fields only is slightly lower than that with fields including the plasma response, no decisive conclusion can be drawn about the relative accuracy of either field model.

2. Fast-ion loss observation

In this experiment, a slowly rotating up/down symmetric (even parity) $n = 2$ magnetic perturbation was applied to a low-elongation ($\kappa \approx 1.16$), low-current ($I_p = 0.6$ MA) L-mode plasma with toroidal field $B_t = 2.0$ T and normalized beta $\beta_N < 1$. The discharge was heated by two separate ≈80 keV neutral beams, one co-current (30L) and the other counter-current (210L). The working gas for the plasma and neutral beams was deuterium. L-mode plasmas were chosen to eliminate additional losses due to ELMs that could complicate analysis of imaging and spectroscopic data. Low elongation was used to make it easier for orbits to intersect the midplane

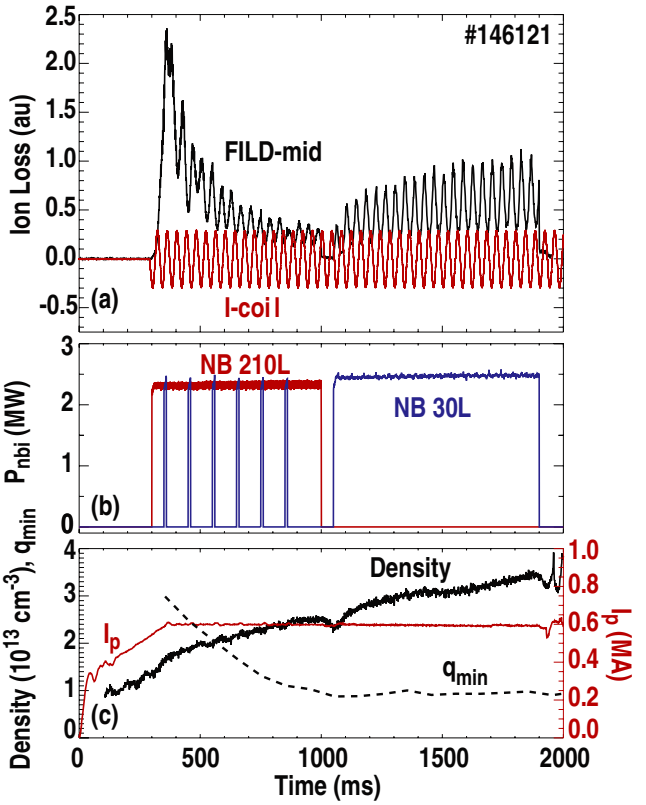

Figure 1. DIII-D Discharge 146121. (*a*) Midplane FILD and I-coil ($\phi = -180°$) timetraces. (*b*) Applied neutral beam waveforms. NB 210L is counter-current and NB 30L is co-current. (*c*) Plasma current (I_p), electron density and minimum safety factor (q_{min}).

FILD detector—with more elongated plasmas, EP losses typically intersect the outer wall well below the midplane FILD. The time history of the relevant signals are given in figure 1. The FILD-mid signal along with the 25 Hz traveling waveform applied to the I-coil at $\phi = 180°$ is shown in figure 1(*a*). The FILD-mid signal clearly exhibits modulation of the fast-ion losses at the I-coil waveform frequency along with several other features. The overall FILD-mid signal is changing dramatically over the time window shown as a result of the beam timing (figure 1(*b*)), current penetration/q-profile evolution and density evolution (figure 1(*c*)). During the first phase of the discharge, the plasma was heated predominantly by the counter-current beam injection (210L) with short blips of the 30L co-current beam for diagnostic purposes. At $t = 1000$ ms, there is a short period during which no beam heating is applied followed by constant injection of only the co-current beam.

The analysis in this paper focuses on the time period near $t = 1000$ ms, an expansion of which is shown in figure 2. Before $t = 1000$ ms, when the 210L beam is being injected, loss to both FILD-mid and FILD-low is observed. After the 50 ms Ohmic phase, the co-current 30L beam begins injection and only loss to FILD-mid is observed. Modulation of losses due to the rotating $n = 2$ perturbation to FILD-mid occurs during both beam phases and an apparent modulation of losses during the 210L phase to FILD-low is also shown in figure 2. Unfortunately, however, inspection of the FILD-low scintillator frames during the 210L phase (not shown)

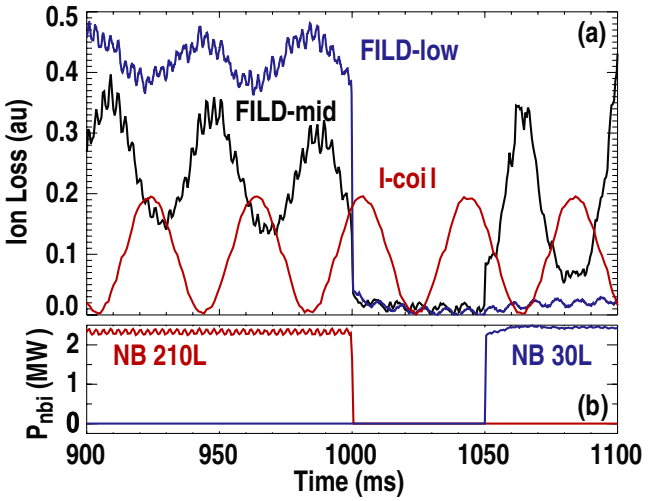

Figure 2. DIII-D Discharge 146121. Expanded region of figure 1. (*a*) FILD-mid, FILD-low and I-coil timetraces. (*b*) 210L and 30L neutral beam waveforms.

exhibit both a strong saturation from large EP fluxes as well as vibration due to the rotating $n = 2$ fields. Vibration of the FILD-low scintillator relative to the camera/PMT viewing optics can cause an apparent oscillation of the PMT signal which is not separable from a modulation of the loss flux. While this has since been remedied for subsequent experiments, FILD-low signals will only be relied upon here to say a much larger loss flux from the 210L beam is observed than the 30L to FILD-low. For these reasons as well as the fact that each probe has a different scintillator response (due to thickness, substrate, and integrated exposure), EP acceptance geometry, slit width, optical train, coupling fibers, etc., no relative calibration between the two FILDs exists and no conclusion should be drawn about the relative signal levels between FILD-mid and FILD-low. The fact that the losses decay almost immediately following turn-off of the 210L beam indicates that the losses are predominantly prompt in nature, i.e. beam neutrals are ionized and hit the FILD detectors within approximately one poloidal transit. In fact, if one zooms in further on the decay, both FILD signals are observed to decay in $<20\,\mu$s after beam turn-off, whereas typical bounce periods are $\approx 40\,\mu$s. Further evidence that the observed loss is prompt, is the fact that small power oscillations in the 210L beam power at 36 Hz show up directly in the measured loss signals. If these signals were due to losses of beam ions that were previously confined or had experienced significant slowing down, these oscillations would, presumably, be washed out. The fact that the FILD signals are dominated by prompt beam ion loss is also consistent with the dependence of the FILD-mid trace in figure 1 on the magnetic geometry. As the current penetrates (q-evolution in figure 1(*c*)), the beam ion confinement becomes better and the prompt loss decays significantly. During this time, however, the density is increasing, and the beam penetration becomes lower causing a shift in the beam deposition to larger radii—something which increases the relative prompt loss to FILD-mid from 30L (see discussion of figure 3).

Having seen that the $n = 2$ modulated fast-ion loss is predominantly a modification of the prompt beam ion loss, reverse orbit tracing of the unperturbed orbits from the FILD-mid location combined with the measured velocity pitch angles can be used to find the approximate birth location and trajectories of the observed ions. Figures 3(*a*) and (*d*) show two typical prompt loss trajectories of full-energy $\approx$80 keV beam ions from the 210L and 30L beams that would be observed at FILD-mid with the measured pitch of $\chi = v_{||}/v = 0.45$ and $\chi = 0.5$ respectively (figures 3(*b*)–(*c*)). These orbits were followed backward in time until they overlapped with the corresponding beam. From figure 3, it is clear that counter beam ions promptly lost to FILD-mid in an unperturbed equilibrium must be born inside the LCFS near mid-radius and co-going beam ions are born outside the LCFS. Thus, to properly model FILD measurements of co-going beam ions in these discharges, beam ionization in the scrape-off-layer (SOL) must be taken into account.

An additional effect resulting from the applied $n = 2$ perturbations that can alter beam ion birth and confinement is a 3D spatial distortion of the kinetic profiles. On the outboard midplane, this is observed as a radial oscillation of the edge density profiles [14, 15] or, as shown in figure 4, the edge bremsstrahlung emissivity. As the I-coil perturbation rotates around the torus, the edge bremsstrahlung profile oscillates radially by $\lesssim$1 cm. This type of oscillation in the edge kinetic profiles can alter the beam ion deposition and can potentially be a source of modulated loss to FILDs or the wall—the next section will discuss how this effect is modeled as well as the perturbed magnetic field impact on the fast-ion orbits.

3. Modeling of fast-ion loss

3.1. Description of model

To model the impact of the applied 3D fields on fast-ion confinement, the problem is broken into three distinct parts: calculation of the perturbing fields and plasma response, calculation of the beam ion birth profile in the presence of perturbed kinetic profiles, full orbit following of the fast-ion trajectories in the equilibrium+perturbed fields and finally collection of these particles at the FILDs and the wall.

The perturbed fields are first calculated using the full coil geometry and currents for the six upper and lower coils at a given timestep ($t = 955$ ms). These fields are then Fourier analyzed toroidally and the $n = 2$ component extracted—referred to as the 'vacuum' $n = 2$ fields. The vacuum fields together with the axisymmetric EFIT [16] calculated magnetic equilibrium and profiles of density, temperature, impurity density, and rotation are used as inputs to the M3D-C1 code [11–13]. M3D-C1 is a resistive two-fluid code which calculates the zero-frequency linear plasma response to the applied 3D fields including perturbed magnetic field, pressure, and density. Profiles of the radial component of perturbed magnetic field for $t = 965$ ms are shown in figure 5, where the perturbed magnetic field including plasma response is shown in figures 5(*a*) and (*b*) and the vacuum $n = 2$ field is given in figures 5(*c*) and (*d*). The fields with plasma response included can be larger than that with vacuum fields only and have significantly more complex structure, particularly near rational

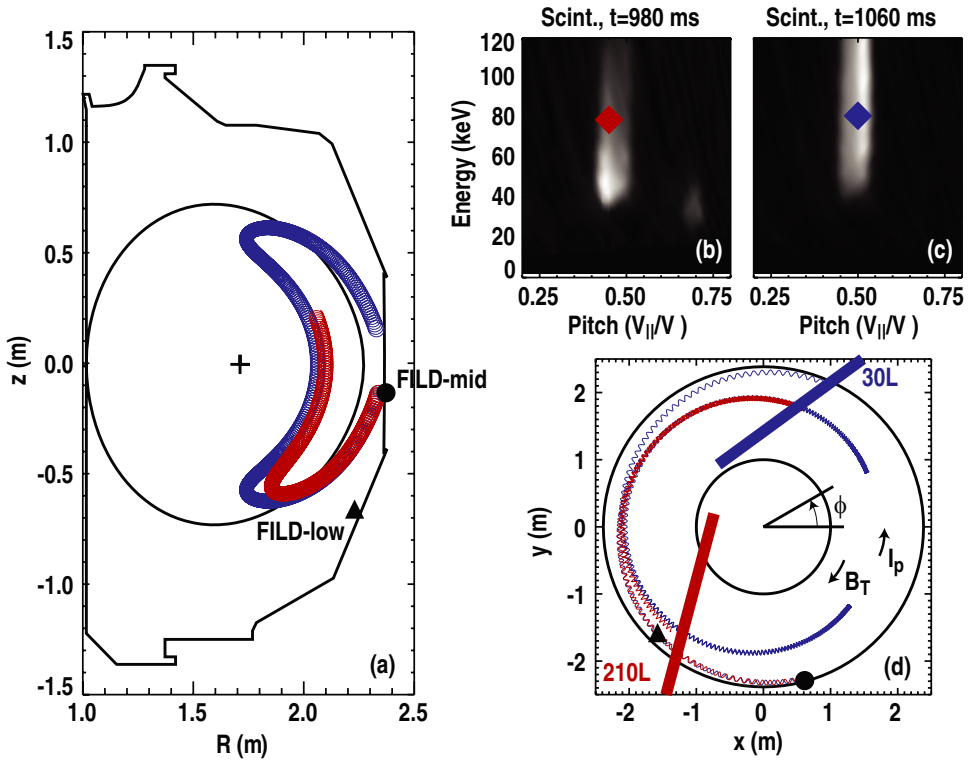

Figure 3. (*a*) Reverse orbit tracing of example full-energy prompt loss orbits from the 210L (red) and 30L (blue) that were detected by FILD-mid. LCFS overlaid as solid line, magnetic axis is '+' symbol. (*b*) FILD-mid scintillator at $t = 980$ ms when 210L beam is on. Red diamond indicates initial energy and pitch ($E = 79$ keV, $\chi = 0.45$) in (*a*). (*c*) FILD-mid scintillator at $t = 1060$ ms when 30L beam is on. Red diamond indicates initial energy and pitch ($E = 81$ keV, $\chi = 0.5$) in (*a*). (*d*) Top-view projection of orbits from (*a*). Diamond indicates position of FILD-low and filled circle represents position of FILD-mid. Beam trajectories for 30L and 210L are also indicated. I_p is counter-clockwise and B_t is clockwise.

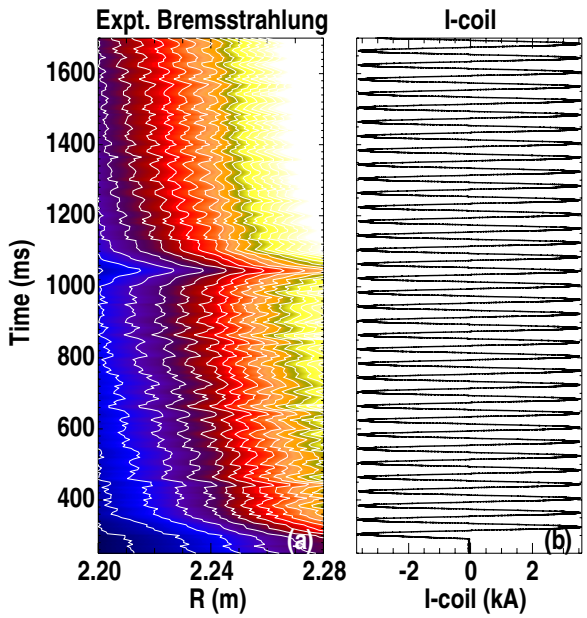

Figure 4. (*a*) Temporal evolution of visible bremsstrahlung emission profile on outboard midplane in DIII-D discharge 146121. White overlaid lines accentuate the radial oscillation. (*b*) Applied I-coil waveform.

surfaces, with peak fields in the plasma of $\delta B/B = 1.4 \times 10^{-3}$ and $\delta B/B = 1.2 \times 10^{-3}$ with and without plasma response respectively.

The beam ion birth profile is calculated using a similar approach to that employed in NUBEAM [17] and FIDASIM [18]. Each beam is broken into several rays on which profiles of density, temperature, and impurity density are interpolated. The attenuation for a given energy and species along each ray is calculated using ADAS beam stopping cross-sections [19] and from this attenuation profile, the probability for birth along a given ray is derived. A Monte Carlo selection process is used to first pick a ray from a given beam, then a position along the ray. For axisymmetric equilibria with attenuation constrained to be zero outside the LCFS, the resulting birth profiles have been compared to those derived from TRANSP/NUBEAM, and no significant disagreement has been found. This module, however, is unique in that it allows arbitrary 3D kinetic profiles such as those from M3D-C1 and naturally includes profiles outside the LCFS. An example full-energy birth profile for the 30L beam is shown in figure 6.

Orbit following is carried out using a FORTRAN based full-orbit solver with fifth order variable step size Runga–Kutta integrator that has been shown to conserve energy and toroidal canonical angular momentum (in axisymmetric fields). Particles from the calculated birth profiles are followed in the presence of the perturbed fields for at least one full poloidal transit and fast ions that come within 5 cm of either FILD detector, with pitch angles capable of being probed ($\chi < 0.8$), are considered to have hit the detector (for reference, the full-energy gyroradius is $R_L = 4$ cm). Particles that cross the DIII-D wall are considered to hit the wall and are not followed past that

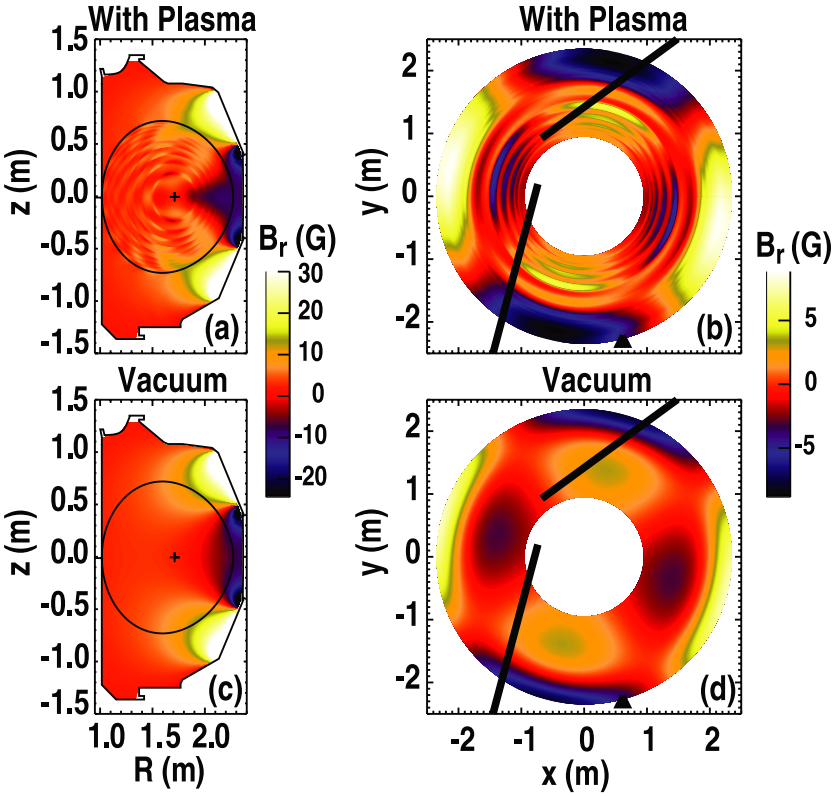

Figure 5. M3D-C1 calculations of the $n = 2$ component of the perturbed radial magnetic field. (*a*) and (*b*) include plasma response. (*c*) and (*d*) are applied vacuum fields only. Top views are through device midplane and when viewed from this perspective, the fields rotate clockwise in the direction opposite to plasma current.

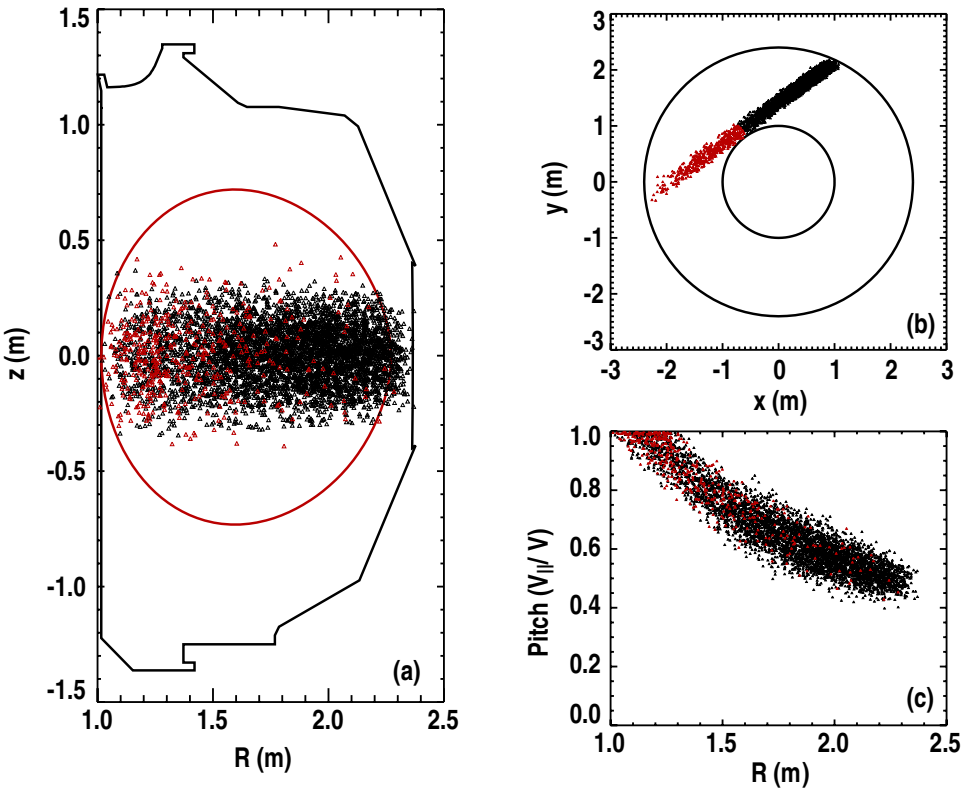

Figure 6. Example birth profile calculation for 30L beam using profiles for 146121 at $t = 965$ ms. (*a*) Birth positions in R, z plane. Red indicates particles born past beam tangency point. Note model includes particles born outside LCFS (shown in red). (*b*) Top view projection of birth locations. (*c*) Pitch of particles at birth position.

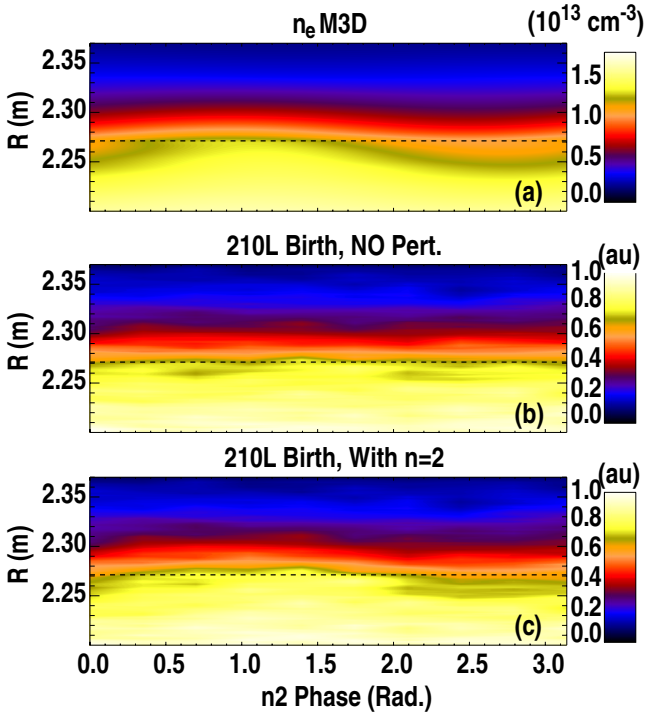

Figure 7. (*a*) M3D-C1 calculations of the perturbed density profile in front of the 210L beamline versus phase of the $n = 2$ perturbation. In (*a*)–(*c*), dashed line represents the unperturbed LCFS from the axisymmetric equilibrium. (*b*) 210L birth profile created by collecting all particles between $|z| < 5$ cm with the $n = 2$ perturbation amplitude set to zero, i.e. NO perturbation. (*c*) 210L birth profile with $n = 2$ perturbation set to experimental amplitude. For (*b*) and (*c*), variation with $n = 2$ phase is from a collection of 10 separate runs with and without the $n = 2$ perturbation respectively.

point. The modeled wall is 3D and includes midplane plane port box cutouts as well as three midplane limiters that protrude approximately 1 cm. To simulate 25 Hz rotation of the $n = 2$ field, the fields are assumed stationary on the timescale of the simulation (O(10–100) μs) and the calculations are repeated for several toroidal phases of the perturbation. These calculations do not include error fields intrinsic to the DIII-D device. Also, collisions are neglected which is warranted given the O(10) ms and O(100) ms for slowing down and 90° pitch angle scattering times, respectively, in the outer half of the plasma.

3.2. Modeling results

Figures 7(*a*) shows the M3D-C1 perturbed density profile on the outboard midplane at $\phi = -120°$, where the 210L beamline enters the vessel, versus phase of the $n = 2$ perturbation ('time'). Similar to the bremsstrahlung measurements shown in figure 4, the density profile exhibits a radial displacement of up to ≈1–2 cm. For reference, in figures 7(*a*)–(*c*), the overlaid dashed line represents the unperturbed LCFS from the axisymmetric equilibrium. Figures 7(*b*) and (*c*) show the 210L beam ion birth profile collected between $-5\,\text{cm} < z < 5\,\text{cm}$ with the $n = 2$ perturbation amplitude set to zero and the experimental level respectively. The calculations in figures 7(*b*) and (*c*) are for ten different phases of the $n = 2$ perturbation and 250*k* particles each. For the case with no perturbation, any variation with phase is due to statistical noise introduced by the finite number of particles. As expected, for the case with the $n = 2$ perturbation included (figure 7(*c*)), there is a clear radial displacement of the birth profile in phase with the density perturbation—shifting the plasma outward causes more fast ions to be deposited at larger radii. It is pointed out that this modulation of the birth profile due to different toroidal phasing of the $n = 2$ perturbation is different than that expected from changes in density profile and so-called density pumpout when 3D fields are first applied. When comparing discharges with and without 3D fields, changes to the $n = 0$ density profile may in fact be more important.

Figure 8 shows the results of several orbit following runs for a variety of field, beam, and birth profile conditions. To identify the major factors contributing to the modulated loss signals, simulations were carried out for both the 210L and 30L beams with no applied 3D field ('NOPert.'), perturbed birth profile but axisymmetric magnetic field, i.e. no $n = 2$ ('δBirth'), unperturbed birth profile but $n = 2$ fields with plasma response included ('δB_{full}'), perturbed birth profile and magnetic field including $n = 2$ contribution with plasma response ('δBirth + δB_{full}'), unperturbed birth profile and $n = 2$ vacuum fields with no plasma response ('δB_{vac}'). Figures 8(*a*)–(*c*) are for 30L beam ion losses and figures 8(*d*)–(*f*) are for 210L beam ion losses. Runs shown in yellow with no perturbation included give an idea of the statistical noise and show the level of prompt losses to the FILDs as well as the total loss to the wall (figures 8(*c*) and (*f*)) in the axisymmetric equilibrium. Adding just the birth profile modification changes the losses to the FILDs slightly but within the statistical noise. However, when orbits are followed in the perturbed equilibrium, clear modulation of the losses to FILD-mid are observed (figures 8(*a*) and (*d*)). Prompt losses to the FILD-low are predicted from the 210L beam ions but not from the 30L beam, as observed experimentally (figure 2). The red curve ('δBirth + δB_{full}') includes all effects and, owing to the rather small impact of the birth profile modification, the predicted FILD signals are very similar to the case with only δB_{full}. If just the vacuum fields with no plasma response are used, a modulation is also apparent, however, the depth of modulation is slightly smaller which is consistent with smaller field amplitudes in the plasma.

As mentioned, the total loss to the wall is also shown in figure 8. For the 30L beam, the total losses (figure 8(*c*)) are similar for all cases with perturbed field included, and, as with the FILD signals, the birth profile modification has a minor impact. For essentially all phases, 30L prompt losses are increased, with the peak increase being ≈7%. For the 210L beam, the total prompt loss level can be influenced by the birth profile modification (blue curve figure 8(*f*)). This can be understood by the fact that, for this counter-current beam, any ion born on the LFS of the magnetic axis within a banana width ($R_B \approx 30$ cm) of the wall will strike it. When the 3D field perturbation is arranged such that the density profile is shifted to larger radii in front of the 210L beam ($n2\text{phase} = 1.1$ in figure 7(*a*)), more fast ions are born closer to the outer wall and the flux to the wall is increased. The total 210L loss change

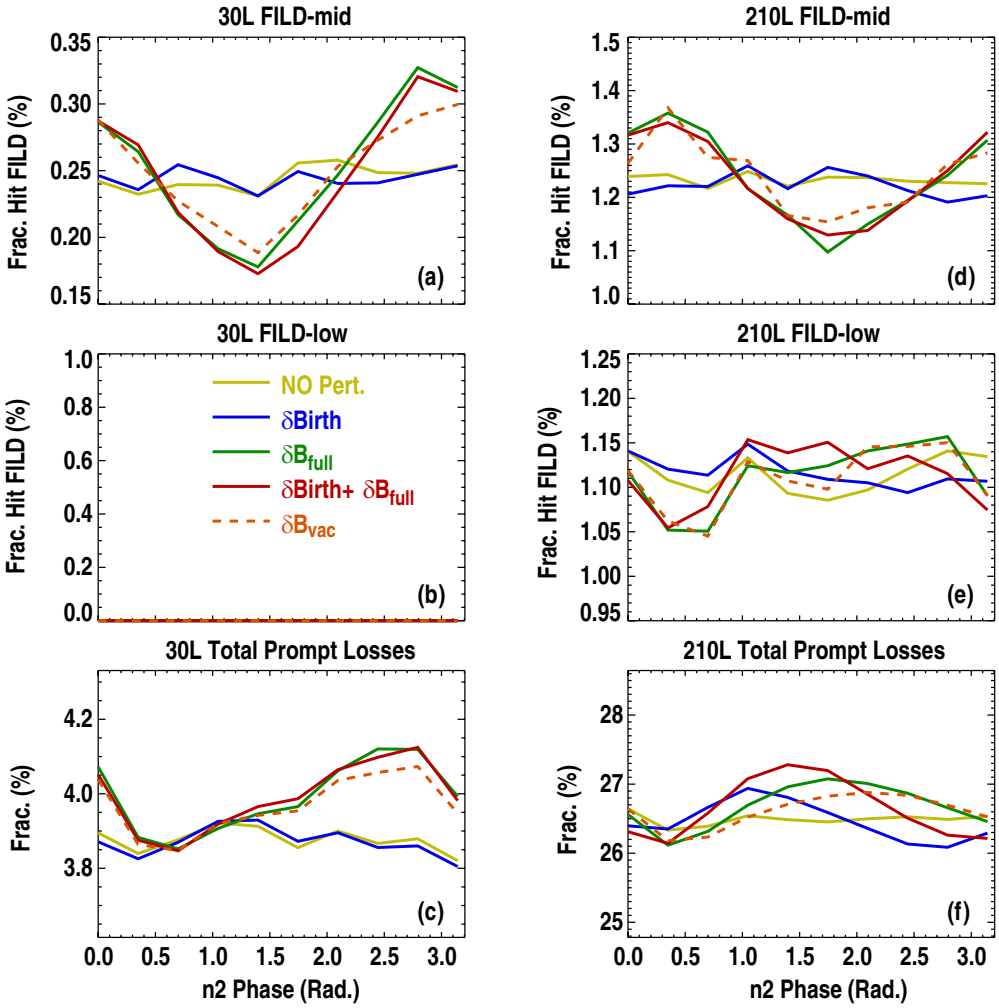

Figure 8. Full orbit following results for full energy 30L (*a*)–(*c*)/210L (*d*)–(*f*)) beams and a range of conditions. Color coding corresponds to: yellow—no applied 3D field ('NOPert.'), Blue—perturbed birth profile but axisymmetric magnetic field, i.e. no $n = 2$ ('δBirth'), green—unperturbed birth profile but $n = 2$ fields with plasma response included ('$\delta B_{\rm full}$'), Red—perturbed birth profile and magnetic field including $n = 2$ contribution with plasma response ('δBirth + $\delta B_{\rm full}$'), Orange dashed—unperturbed birth profile and $n = 2$ vacuum fields with no plasma response ('$\delta B_{\rm vac}$'). (*a*) and (*d*) Fraction of launched particles coming within 5 cm of FILD-mid. (*b*) and (*e*) Fraction of all launched particles coming within 5 cm of the FILD-low. (*c*) and (*f*) Fraction of all launched particles lost to the wall.

is then a compromise between the birth profile modification of the loss and that due to the fields which are maximized at different phases. No birth profile dependence occurs for the 30L beam because the prompt losses are dominated by passing particles born near the beam on the HFS of the magnetic axis, where the birth profile is relatively unperturbed.

The modulation of the signal at the midplane FILD can be explained by looking at the trajectories of the unperturbed and perturbed orbits, an example of which is shown in figure 9 for a typical 30L injected fast ion. The simulations show that the perturbed orbits are displaced by approximately $\approx$1 cm radially from their unperturbed trajectories. For toroidal phase of the $n = 2$ perturbation $\delta\phi = 2.8$, the trajectory is pushed out on its first banana orbit and strikes FILD-mid. For $\delta\phi = 1.4$, the orbit is displaced inward from its unperturbed orbit on its first poloidal transit and eventually strikes the wall later at another location on a subsequent poloidal transit. One phase pushes particles toward FILD-mid, another pushes them away. The tips of the perturbed banana orbits are observed to move vertically from the axisymmetric case, indicating magnetic moment is conserved in this process.

To compare the experimental data directly to simulation, the midplane FILD data are mapped from time to the equivalent phase of the $n = 2$ perturbation used in the simulations and scaled by the average FILD-mid signal over one cycle—the results of which are shown in figure 10. The modeling results in figure 10(*b*) are those from figures 7(*a*) and (*c*) that include both the perturbed birth profile and $n = 2$ magnetic field with plasma response (i.e. 'δBirth + $\delta B_{\rm full}$'). Modeling captures many of the features apparent in the FILD-mid data: larger modulation of 30L losses as compared to 210L, 30L losses peak near $n2\text{phase} = 0$, and an approximate 30° phase shift between 30L and 210L loss modulation is also observed as in experiment. The depth of modulation from simulation, however, is smaller than that observed experimentally. There are several potential reasons for this disagreement, the first is that the modeling includes only the $n = 2$ contribution to the perturbed magnetic fields. Due to the finite number of coils in each row (six) there is a significant $n = 4$ contribution that, in

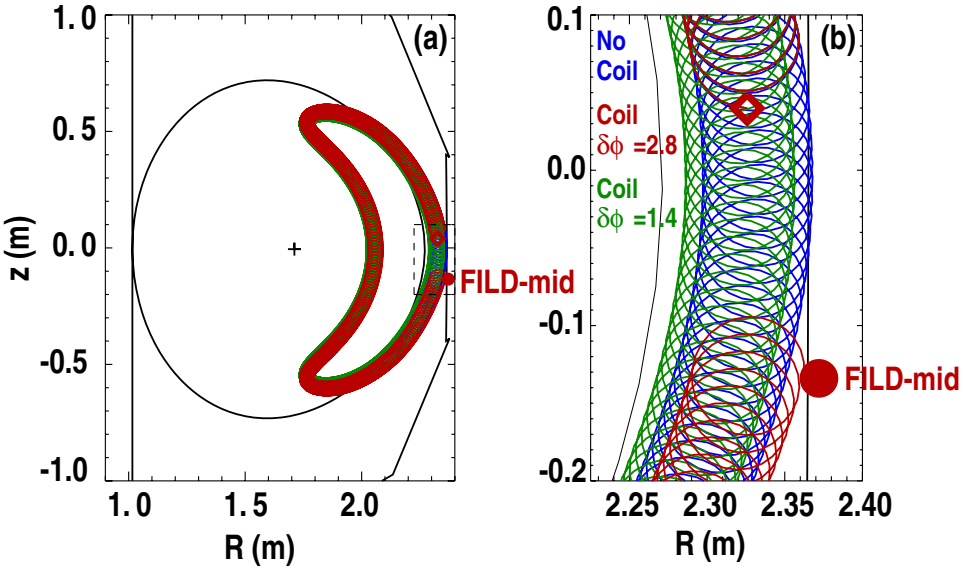

Figure 9. (*a*) Example 30L orbits initialized at the position represented by the red diamond. Blue = no $n = 2$ perturbation, Red includes the $n = 2$ fields with $n2$phase = 2.8 rad, green is with $n = 2$ perturbation phase = 1.4 rad. Red corresponds to phase at which flux of particles striking FILD is maximized. (*b*) Zoomed in region of (*a*).

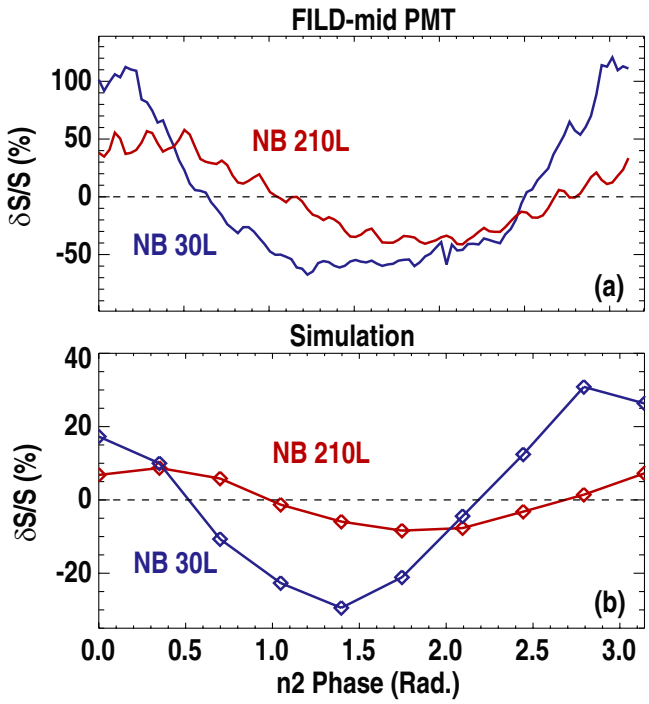

Figure 10. DIII-D Discharge 146121. (*a*) FILD-mid PMT data from 30L (blue) and 210L (red) mapped equivalent phase of the $n = 2$ perturbation. Data from 40 ms interval centered at $t = 965$ ms and $t = 1070$ ms for the 210L and 30L beams respectively. Data are expressed as the difference from the mean (δS), divided by the mean (S) over the 40 ms interval. (*b*) Simulation results for expected modulation. Simulations are the same as shown in figure 8 for ('δBirth + δB_{full}').

vacuum, can be up to half the amplitude of the $n = 2$ fields. An indication that this may be significant is apparent in the 30L FILD-mid data in figure 10(*a*), where the modulation is clearly asymmetric about the mean and not sinusoidal as the modeling predicts. Another factor that can contribute to the difference is that the FILD-mid data include losses from full, half, and third energy components whereas modeling has only been carried out for the full-energy component of the losses. Simulations were also run for 4× the duration of those shown in figure 10 to check whether including more bounce periods could change the depth of modulation with the result that no significant difference was found.

As shown in figures 8(*c*) and (*f*), the total loss to the wall for each beam is altered by the application of the $n = 2$ fields. In addition to the total lost number of particles, the position at which the particles strike the wall is recorded in the simulations. For each phase of the I-coil perturbation these strike positions are collected and a 2D map of the wall heat load is constructed. Figures 11(*a*) and (*e*) show the wall heat load averaged over a $n = 2$ rotation cycle on the outboard wall for the 210L and 30L beams. Wall heating is expressed in terms of the fraction of full-energy particles launched per unit area on the wall—the 210L/30L beams injected 1.7 MW and 1.8 MW, respectively in the full-energy components. These figures show the 210L counter beam causes approximately 10× the peak heat flux of the co-injected 30L beam. Rectangular discontinuities in the heat footprint between ±20° poloidally are due to port box cutouts and limiters (shown as dashed rectangles). Preferential heating is, as expected, observed on the side of port boxes in the direction of the plasma current due to the fact that almost all losses occur on the co-current leg of orbits. A small fraction of particles born within a Larmor radius of the wall are lost within one gyro-period and can be seen as hotspots near $\phi \approx -125°$ and $\phi \approx 70°$ for the 210L and 30L beams respectively. The FILD-mid and FILD-low locations are also shown in these figures (diamonds), making it obvious that the 210L prompt losses should be observed on both FILDs whereas the 30L should only be seen on FILD-mid. By taking the difference with the 'no coil' case, the areas of increased average heat load due to the coil perturbation can be found, and the results are given in figures 11(*b*) and (*f*). In both cases, there are several areas of increased localized heating, particularly near the midplane region. By fitting the

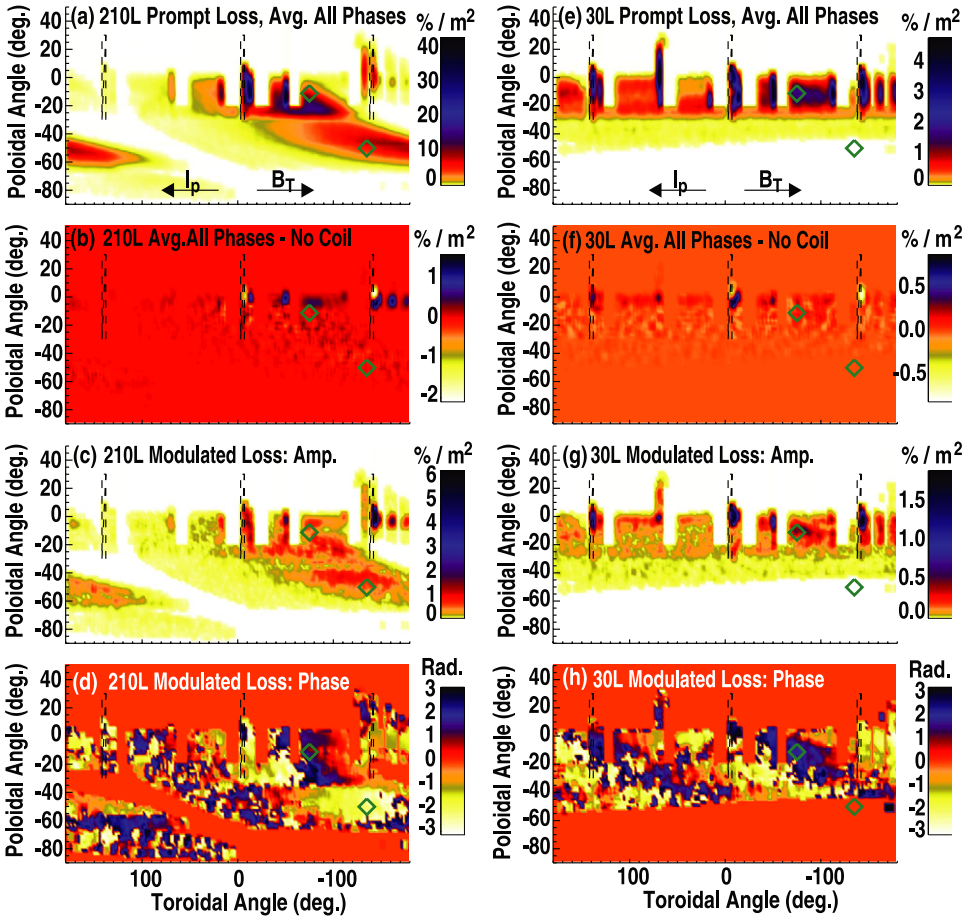

Figure 11. Simulation results obtained by histogramming losses to wall. Dashed rectangles represent location of limiters. Green diamonds are the FILD positions. (*a*)–(*d*) 210L beam loss information. (*a*) Average loss flux averaged over all phases of $n = 2$ perturbation. (*b*) Difference of (*a*) with the 'no coil' case. (*c*) Amplitude of the modulated signal (A) from fitting the lost ion flux each wall position by $I = A\sin(2\phi_{n2} + \alpha) + b$. (*d*) Phase of the modulated signal (α). (*e*)–(*h*) 30L beam loss information. Note, wall fluxes expressed in terms of fraction of launched full-energy particles.

loss versus phase of the $n = 2$ perturbation for each position on the wall with a DC offset sine wave, the amplitude and phase of the modulated loss to the wall due to the rotating perturbation can also be found. The amplitude of the periodic modulation for the two beams are given in figures 11(*c*) and (*g*) and the phase in figures 11(*d*) and (*f*). The modulated heat flux to the wall has a very similar pattern to the prompt loss/average heat flux shown in figures 11(*a*) and (*e*) and is largest near the limiters, particularly for the 30L beam. Comparison of the amplitude and phase of the losses, as in figure 10, is a powerful tool for validation and to expand upon the highly localized FILD measurements shown here, these simulations will eventually be directly compared to measurements with a wide field-of-view infrared imaging system recently installed on DIII-D [20].

4. Conclusions and future work

In this article, measurements and modeling of prompt beam ion loss modulation by applied rotating $n = 2$ fields with $\delta B/B \approx 10^{-3}$ in an L-mode plasma were presented. Scintillator data show that the applied fields are capable of modulating the local beam ion prompt loss flux to a given FILD by up to 100% about the mean, depending on the toroidal phase of the perturbation. Detailed modeling of these experiments has been carried out using M3D-C1 calculations for the perturbed kinetic profiles and magnetic fields combined with beam deposition and full-orbit following codes. The predicted phase of the modulated loss signal with respect to the I-coil currents is in close agreement with FILD measurements as is the relative amplitudes of the modulated losses for the co- and counter-current beam used in the experiment. Of the simulations carried out, the case which includes the full plasma response and larger modulation of the losses, due to larger peak fields in the plasma, is in slightly better agreement with measurements than that with vacuum $n = 2$ fields only. The predicted peak-to-peak modulation of the losses is lower than measured experimentally, potentially due the neglect of a significant $n = 4$ component in the applied fields. Changes in edge density for different phases of the perturbation modify the birth profile and consequent prompt losses but, for the case investigated, the perturbed magnetic field has a larger effect on the modulated losses. These simulations also show that the total prompt loss flux to the wall can be increased by up to 7% depending on injection geometry and phase of the applied perturbation.

The realization that the dominant feature observed on fast-ion loss detectors is due to a modification of prompt beam ion loss is important when looking toward future devices such as ITER. For modeling those devices, to properly capture the relevant orbits, the correct beam injection geometry relative to the field perturbation and neutral beam ionization in the scrape-off layer must be included. As mentioned above, the relative phase of the birth location and perturbed field can have a significant impact on the loss levels and wall heating. For the discharge discussed here, the applied 3D field was on continuously for the period of interest and an $\approx$1 cm radial oscillation in beam ion birth profile was inferred due to the non-axisymmetric, rotating, density perturbation. For discharges with significant density pumpout upon application of 3D fields, where pedestal densities can change by up to 30% [21], it is expected that this will have an even larger impact on the beam ion birth profile. Self-consistent beam ion birth profiles with and without the perturbation should be used when evaluating the fast-ion loss due to the applied perturbation.

Future work will include multiple toroidal mode numbers in the simulations. Additionally, long timescale simulations targeting the impact of the applied 3D fields on the confined fast-ion distribution are underway; these simulations are being carried out with the SPIRAL full-orbit code [22] and include pitch-angle scattering as well as slowing down. These simulations will be compared to fast-ion D-alpha (FIDA) measurements of the confined fast-ion profile as well as additional FILD-mid measurements that show some indication of losses that are non-prompt in nature—in fact, the very low amplitude loss spot in figure 3(*b*) at $\chi \approx 0.7$ and $E \approx 40$ keV is one such example in that it decays over 15 ms. Comparisons of the wall heat load calculations with wide field-of-view infrared imaging measurements are also planned. To help address the validity of various 3D field models for modeling of future devices, new DIII-D experiments will study discharges where the plasma response to the non-axisymmetric fields has a significant effect on the modulated prompt losses.

Acknowledgments

This work was supported in part by the US Department of Energy under DE-FC02-04ER54698, SC-G903402, DE-AC02-09CH11466, DE-FG02-04ER54761 and DE-FG02-05ER54808. Effective beam stopping cross-sections used in the beam ion birth profile calculations were obtained from the Atomic Data and Analysis Structure (ADAS) compilation. The originating developer of ADAS is the JET Joint Undertaking.

References

[1] Spong D A 2011 *Phys. Plasmas* **18** 056109
[2] Shinohara K *et al* 2011 *Nucl. Fusion* **51** 063028
[3] Heyn M F, Ivanov I B, Kasilov S K, Kernbichler W, Loarte A, Nemov V V and Runov A M 2012 *Nucl. Fusion* **52** 054010
[4] Koskela T, Asunta O, Hirvijoki E, Kurki-Suonio T and Äkäslompolo S 2012 *Plasma Phys. Contol. Fusion* **54** 105008
[5] Tani K, Shinohara K, Oikawa T, Tsutsui H, Miyamoto S, Kusama Y and Sugie T 2012 *Nucl. Fusion* **52** 013012
[6] Asunta O, Akasiompolo S, Kurki-Suonio T, Sipila S, Snicker A, Garcia-Munoz M and the ASDEX Upgrade Team 2012 *Nucl. Fusion* **52** 094014
[7] Garcia-Munoz M *et al* 2013 *Nucl. Fusion* **53** 123008
[8] Fisher R K, Pace D C, Garcia-Munoz M, Heidbrink W W, Muscatello C M, Van Zeeland M A and Zhu Y B 2010 *Rev. Sci. Instrum.* **81** 10D307
[9] Pace D C, Fisher R K, Garcia-Munoz M, Darrow D S, Heidbrink W W, Muscatello C M, Nazikian R, Van Zeeland M A and Zhu Y B 2010 *Rev. Sci. Instrum.* **81** 10D305
[10] Chen X, Fisher R K, Pace D C, Garcia-Munoz M, Chavez J A, Heidbrink W W and Van Zeeland M A 2012 *Rev. Sci. Instrum.* **83** 10D707
[11] Ferraro N M and Jardin S C 2009 *J. Comput. Phys.* **228** 7742
[12] Ferraro N M 2012 *Phys. Plasmas* **19** 056105
[13] Ferraro N M, Lao L L, Evans T E, Moyer R A, Nazikian R, Orlov D M, Shafer M W and Unterberg E A 2012 *Proc. 2012 IAEA Fusion Energy Conf. (San Diego, CA)* paper TH/P4-21
[14] Moyer R A *et al* 2012 *Nucl. Fusion* **52** 123019
[15] Stoschus H *et al* 2012 *Nucl. Fusion* **52** 083002
[16] Lao L L, St John H E, Stambaugh R D, Kellman A G and Pfeiffer W 1985 *Nucl. Fusion* **25** 1611
[17] Alexei P, Douglas M, Robert A, Glenn B and Arnold K 2004 *Comput. Phys. Commun.* **159** 3
[18] Heidbrink W W, Liu D, Luo Y, Ruskov E and Geiger B 2011 *Commun. Comput. Phys.* **10** 716
[19] Atomic Data and Analysis Structure (ADAS) compilation. *ADAS* http://adas.phys.strath.ac.uk
[20] Lasnier C J, Allen S L, Fenstermacher M E A, Hill D N and Weber T R 2011 *Bull. Am. Phys. Soc.* **56** 169
[21] Unterberg E A, Evans T E, Maingi R, Brooks N H, Fenstermacher M E, Mordijck S and Moyer R A 2009 *Nucl. Fusion* **49** 092001
[22] Kramer G J, Budny R V, Bortolon A, Fredrickson E D, Fu G Y, Heidbrink W W, Nazikian R, Valeo V and Van Zeeland M A 2013 *Plasma Phys. Control. Fusion* **55** 025013